JOURNAL OF SOLID STATE CHEMISTRY 49, 25–42 (1983)

Microstructure and Microanalysis of Bismuth Molybdates

P. L. GAI

Department of Metallurgy and Science of Materials, University of Oxford, Parks Road, Oxford OX1 3PH, United Kingdom

Received November 8, 1982; accepted in revised form March 22, 1983

The microstructures of commercially important bismuth molybdate catalysts in relation to olefin oxidation reactions are examined by electron microscopy (EM) techniques. The microstructural characterization has been carried out using dynamic (*in situ*) EM, high resolution EM, and microanalysis. The coprecipitated catalyst system Bi_2MoO_6 or γ, together with the γ phase, contains small amounts of tetragonal Bi_2MoO_6 phase, $Bi_2Mo_3O_{12}$ (α phase), Bi_2O_3, and MoO_3. In reduction with propylene, at catalyst operating temperatures of 400–500°C, in the dynamic experiments conducted on α- and γ-phase crystallites under reaction conditions no evidence for extended defects such as crystallographic shear planes has been obtained, instead an ordered intermediate phase similar to (101) $Bi_2Mo_2O_9$ (β phase) is observed which is found to be unstable. Observations by electron microscopy have been confirmed with parallel measurements made in a reactor connected to a gas chromatograph and mass spectrometer system. The possible influence of the microstructural changes on the catalytic behavior of the system is examined.

Introduction

Heterogeneous catalysis has played a major role in the development of petrochemical industry as is well known. The bismuth molybdate-based system is one of the most important heterogeneous catalyst systems used for the selective oxidation and ammoxidation of olefins which account for the production of a substantial portion of key industrial chemicals. The present era of olefin oxidation progressed dramatically with the discovery of bismuth molybdates as oxidation catalysts because of their high selectivity (over 90%) and activity (*1, 2*), and now form the basis of the commercial catalysts. Detailed solid state structural work on the system has revealed three major phases in the *active* region of the phase diagram: $Bi_2Mo_3O_{12}$ (α phase), $Bi_2Mo_2O_9$ (β), and Bi_2MoO_6 (γ). The activity and selectivity of catalyst systems, however, are known to depend upon the changes in their microstructure, and despite extensive chemical studies such changes in the complex multiphase Bi–Mo–O system are not clearly understood. Differences of opinions exist about the reactivity of various phases; the nature of the active phase during reactions and structures of many phases occurring in the system are still to be finalized. It is likely that the conventional X-ray diffraction methods may not always be useful in detecting many of the microstructural changes and the presence of minor phases present, and postreaction examination of the static catalyst does not always represent the dynamic catalyst (under reacting conditions). With these aspects in mind, electron microscopy (EM) techniques such

0022-4596/83 $3.00

as the *in situ* (dynamic) EM, high resolution EM (HREM), and microanalysis have been applied in this paper in the systematic studies of the complex bismuth molybdate system to obtain microstructural information at high resolution and to gain an insight into the mechanisms of operation. *In situ* EM is used to examine directly the mechanisms of reactions (e.g., redox) as a function of temperature, gas environments (e.g., hydrocarbon; hydrocarbon + oxygen mixtures), nucleation of defects/phases, presence of unstable intermediate phases, catalyst degradation, and reoxidation. The microstructures are further examined by HREM with a point resolution of ~1.7 Å.

Although the industrial catalysts contain bismuth molybdates supported on, e.g., alumina or silica, many fundamental studies employ unsupported catalysts initially to understand the basic issues governing selectivity, activity, and microstructural changes. Accordingly, in the present paper results relating mainly to unsupported bismuth molybdates using the EM methods have been reported. The microstructural characterization has been complemented where necessary, by local chemical composition analysis by analytical EM (AEM) and electron probe microanalysis (EPMA).

Experimental Procedures

(*a*) *Sample preparations*. Bismuth molybdates using the proportions (1) $Bi_2O_3 \cdot 3MoO_3$ (α), (2) $Bi_2O_3 \cdot 2MoO_3$ (β), and (3) $Bi_2O_3 \cdot MoO_3$ (γ) were prepared by the coprecipitation method and also by solid state fusions of the oxides. In the coprecipitation method, aqueous bismuth nitrate and ammonium paramolybdate were used and the powders were calcined at temperatures between 500 and 550°C according to the procedures described by Batist *et al.* (*3*). The coprecipitation catalysts are used in industry because they offer a combination of high surface area, high reactivity, and selectivity as well as good thermal stability. The solid state samples were also calcined at temperatures similar to those described above. Single-phase crystals were grown where possible (*4*).

(*b*) *Electron microscopy*. The *in situ* experiments were carried out in a gas reaction cell (*5*) fitted to an AEI-EM7 high voltage electron microscope (HVEM) operating at an accelerating voltage of 1 MeV. With this technique, realistic gas pressures (up to 1 atm) and temperatures (up to 1000°C) may be used in the gas reaction cell and dynamic events may be recorded either on photographic films or on a video system coupled to an image intensifier using very low beam currents (*6, 7*). Blank experiments (without the beam) were also performed in each case to confirm the direct observations.

Reduction experiments were carried out *in situ* in continuous flows of propylene (C_3H_6, and alternatively in C_3H_6–NH_3 gases or 10% H_2 diluted with helium, supplied by British Oxygen) usually at a total pressure of 100 Torr. Reactions were also performed in C_3H_6–O_2 mixtures. Parallel experiments were conducted under identical conditions on larger amounts of similar samples (~0.5-2 g) supported between plugs of glass wool in a microreactor (fixed bed) fitted to a Varian 3700 gas chromatograph (GC) interfaced with a Vacuum Generators (VG) Q7B quadrupole mass spectrometer (MS) and controlled by an Apple microcomputer. The samples were examined in 100- to 200-keV EMs to conform the direct observations. Preliminary experiments were also carried out to monitor the activity of the coprecipitated samples in the microreactor with the GC–MS system by passing pulses of C_3H_6 at ~5-min intervals in N_2 carrier gas (with flow rates between 20 and 30 cm^3/min) (*8*).

The microstructural characterization was further carried out at high resolution using a JEOL JEM 200CX EM at 200 keV with a point resolution of ~1.7 Å and a CTF first

zero at 2.4 Å at optimum defocus (*9*). The high resolution phase contrast lattice images from crystallites were checked against the simulated images using the programs incorporating the multislice methods of the dynamical theory of electron diffraction (e.g. (*10*)).

The local chemical composition from thin crystallites was obtained by AEM using the Oxford field emission gun STEM (for crystallites with diam. <1000 Å) and by EPMA using an automated Cameca microprobe fitted with energy dispersive and wavelength dispersive spectrometers (EDS and WDS) for larger crystallites (0.25 μm to a few micrometers). In EPMA, analyses were carried out between 5 keV-20 keV using compound standards of $Bi_2Mo_3O_{12}$ and Bi_2MoO_6 samples which had been characterized by X-ray and electron diffraction methods. Concentrations of Bi and Mo of reacted crystallites were determined by measuring the intensities of M_α and L_α lines of Bi and Mo and the oxygen content was analyzed by difference. Quantitative corrections of spectra were carried out using the CORREX files in the standard MBXCOR programs (for details see, Refs. (*11, 12*)).

Results

Structural Investigations by HREM

The samples were examined by HREM to obtain microstructural information regarding various phases that exist in the coprecipitated system. The γ-Bi_2MoO_6 (or γ-2BiMo) preparation is described in detail here. The fresh preparation contained γ as the main phase. The high resolution lattice image and the electron diffraction pattern of γ-Bi_2MoO_6 in (100) projection recorded at 200 keV are shown in Figs. 1a and b. Some contrast anomalies (indicative of point defects) are shown by arrows in Fig. 1a. The images were recorded at an electron microscope defocus setting (Δf) of -700 Å (near the optimum defocus) with an objective aperture out to ~0.6 $Å^{-1}$. The experimental defocus was determined by using the minimum contrast at zero focus as a reference or by carbon contamination. The structure of this low temperature modification is similar to that of the natural mineral koechlinite (Bi_2MoO_6) described by Zemann (*13*) and later refined by Van den Elzen and Rieck (*14*) and has a = 5.487 Å, b = 16.22 Å, c = 5.506 Å, orthorhombic, space group $Pca2_1$ and Z = 4.

The structure consists of layers of $(Bi_2O_2)^{2+}$ units and $(MoO_2)^{2+}$ units interconnected by O^{2-} ions. The O^{2-} and the $(MoO_2)^{2+}$ unit form distorted $(MoO_4)^{2-}$ layers. The atomic structure and the electron diffraction calculated using the structure data of Van den Elzen and Rieck (*14*) are shown in Figs. 1c and d, respectively, and d-spacings from the latter are consistent with those from the observed image. The simulated lattice images were found to be very sensitive to defocus and thickness conditions. A calculated image is inset in Fig. 1a for a crystal thickness (t) of ~100 Å. Fig. 1(e) shows an SEM micrograph of crystallites in the catalyst system.

The HREM of the coprecipitated sample also revealed the presence of small amounts (about 1–2%) of tetragonal Bi_2MoO_6 phase hitherto believed to exist only at the high temperature of ~750°C. The nature of the phase was confirmed by lattice images and electron diffraction patterns shown in Figs. 2a and b, respectively, in (010) projection. The tetragonal phase has lattice parameters of a = 3.95 Å, c = 17.21 Å (space group D_{2d}^{11}, $I\bar{4}2m$), and Z = 2 (Blasse (*15*)) and is isostructural with La_2MoO_6 (*16*). According to Blasse (*15*), the structure differs from koechlinite in one aspect and that is the MoO_4 layer consists of MoO_4 tetrahedra with no anions common. The Bi_2O_2 layers and Mo positions are unaltered; only anions in MoO_4 layers are rearranged, but Matsuura *et al.* (*17*) consider

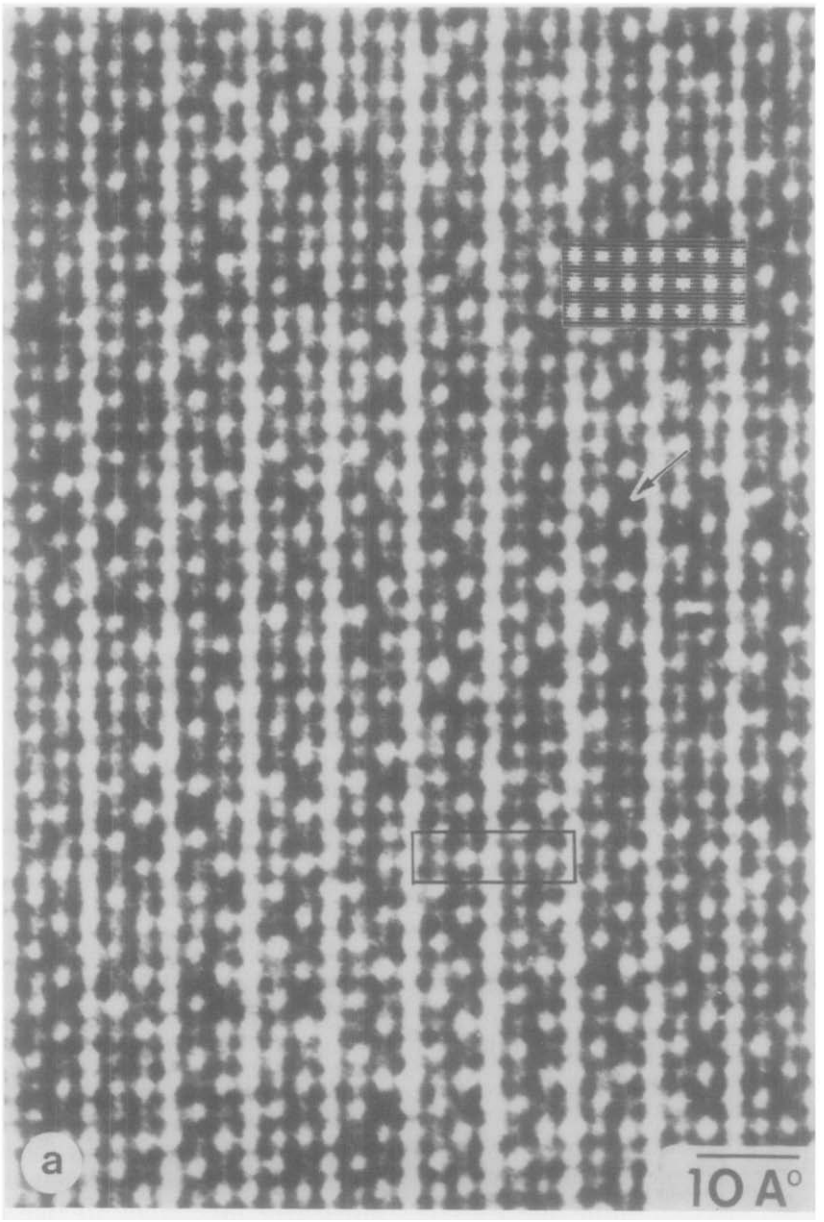

FIG. 1. (a) High resolution lattice image of γ-Bi_2MoO_6 in (100) projection at 200 keV. Dark regions represent contrast from metal atoms. (b) Electron diffraction pattern (the samples were found to be beam sensitive). (c) Atomic projection of γ in (100). (d) Calculated electron diffraction pattern in (100). (e) An SEM micrograph of the microcrystalline powder catalyst.

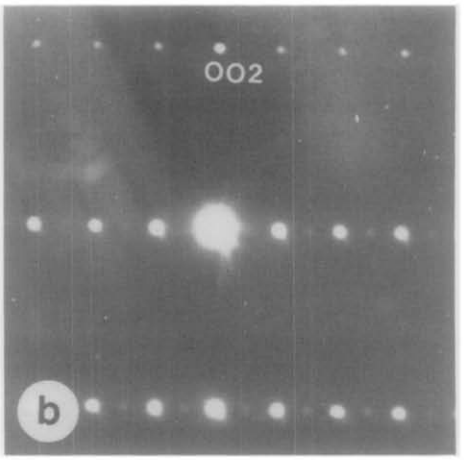

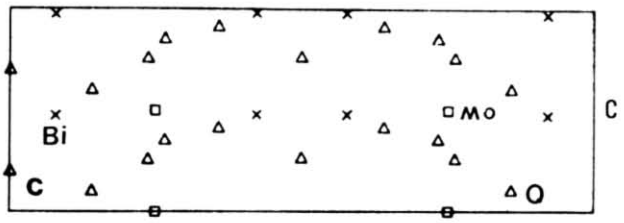

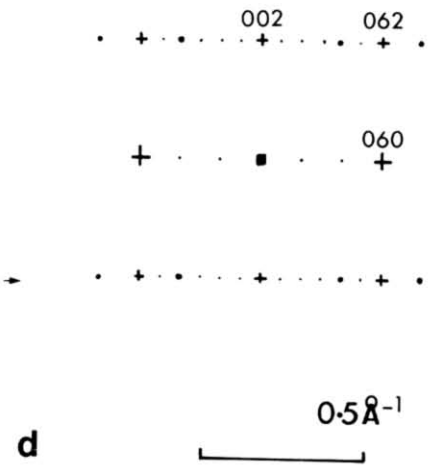

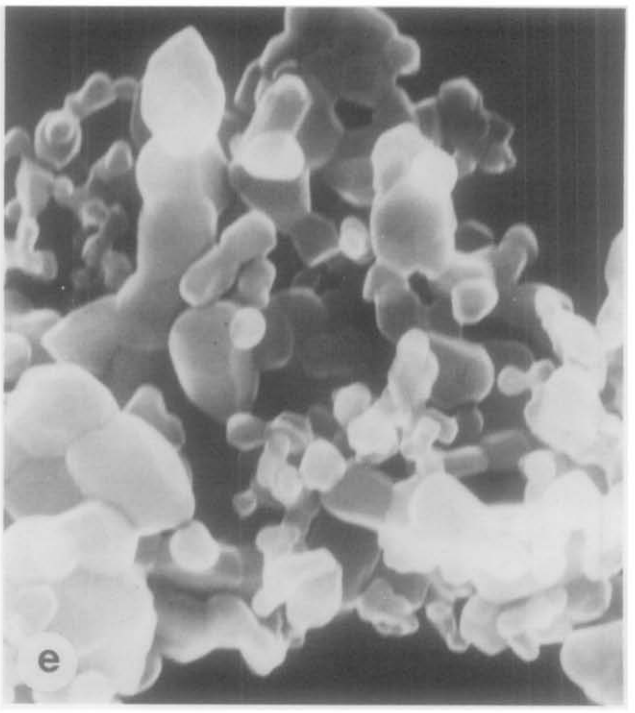

FIG. 1—*Continued.*

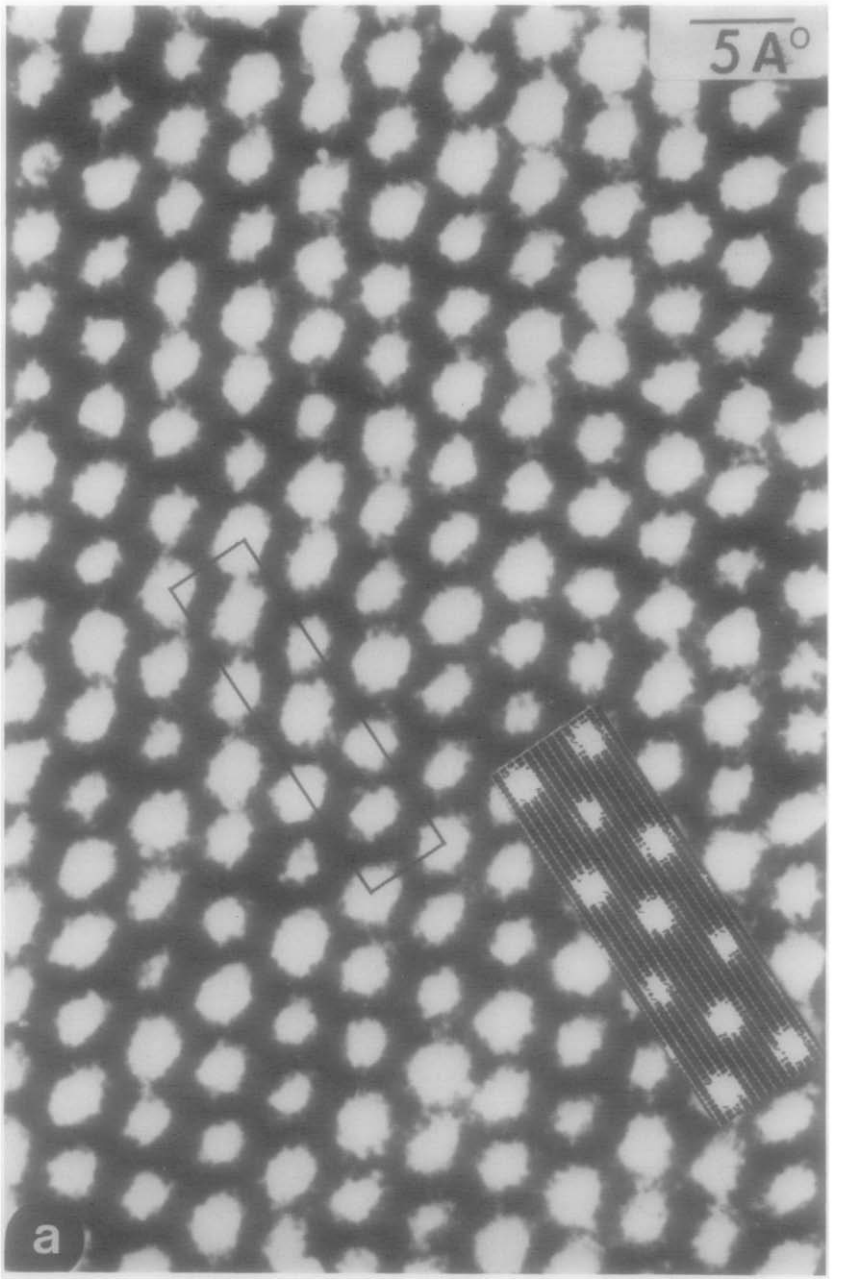

FIG. 2. (a) Lattice image of tetragonal Bi_2MoO_6 in (010) projection with simulated image inset. The unit cell is outlined. (b) Electron diffraction pattern in (010).

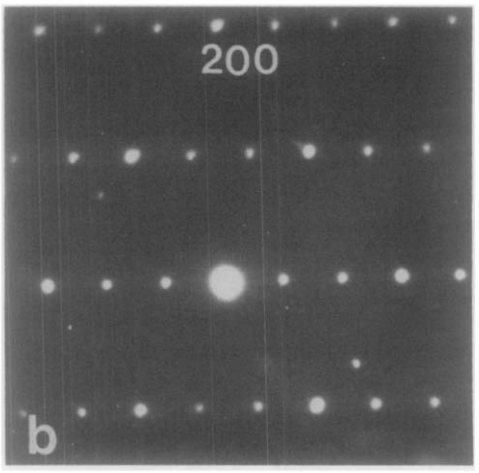

FIG. 2—*Continued.*

the structure to be more similar to the α-($Bi_2Mo_3O_{12}$) structure due to different MoO_4 configurations. Nevertheless, ignoring the differences in the MoO_4-type layers, the structure image was stimulated based on the data by Blasse and is inset in Fig. 2a for $\Delta f = -800$ Å and for $t \sim 40$ Å. The agreement between the images is satisfactory. Small amounts of the α phase were also detected in the preparations.

The coprecipitated $Bi_2O_3 \cdot 3MoO_3$ samples contained $Bi_2Mo_3O_{12}$ (α phase) as the main phase together with small amounts of γ. The α phase is monoclinic with $a = 7.68$ Å, $b = 11.491$ Å, $c = 11.929$ Å, $\beta = 115.4°$, space group $P2_1/C$, and $Z = 4$ (*18*) and is closely related to the mineral scheelite (*19*). The perfect scheelite ($CaWO_4$) structure (with general formula AMO_4; M is a tetrahedral cation and A is a cation bonded to eight oxygens) is shown in Fig. 3a in (001) projection where ○ = cations and ◇ = MoO_4 tetrahedra. The distorted structure may be written as $Bi_{2/3}\phi_{1/3}MoO_4$ where ϕ are ordered bismuth vacancies and the projection is shown in Fig. 3b after Sleight (*19*). The shaded units are top layers and the unshaded units are quarter of the way down the unit cell. Each Bi ion has eight oxygen neighbors and Mo occurs in pairs of polyhedra sharing edges (Mo_2O_8), thus being a distorted tetrahedra with a fifth oxygen situated at a greater distance. The structure image of α (010) is shown in Fig. 4a, with the projection of the atoms in the unit cell in Fig. 4b.

Some crystallites in both the preparations were identified as Bi_2O_3 (α modification) and MoO_3 by electron diffraction, lattice imaging, and microanalysis.

Activity Studies of the Coprecipitated γ

The conversion of C_3H_6 was determined with respect to the catalyst reduction by passing C_3H_6 over the catalysts (with surface area ~4 m^2/g) in the microreactor and monitoring the products at a temperature of ~450°C (near the operating temperature). The chart shown in Fig. 5 reveals several stages of activity variations and the activity begins to decrease somewhat after ~1 hr. A drop in selectivity to acrolein (i.e., the percentage of consumed C_3H_6 converted to acrolein), was also observed above ~450°C. The samples at stages A, B, C, and D were examined immediately after the reactions by electron microscopy.

Sample A (fresh sample) contained γ-2BiMo, tetragonal phase, small amounts of

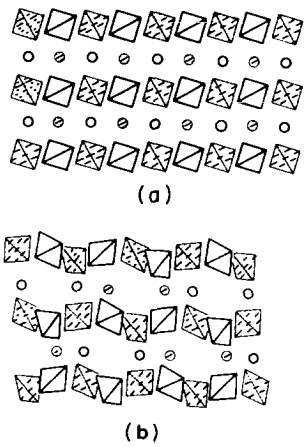

FIG. 3. Structure down the c axis of (a) pure scheelite, (b) $Bi_2Mo_3O_{12}$ (α) showing vacant cation sites. ○ = cations, ◇ = MoO_4 tetrahedra.

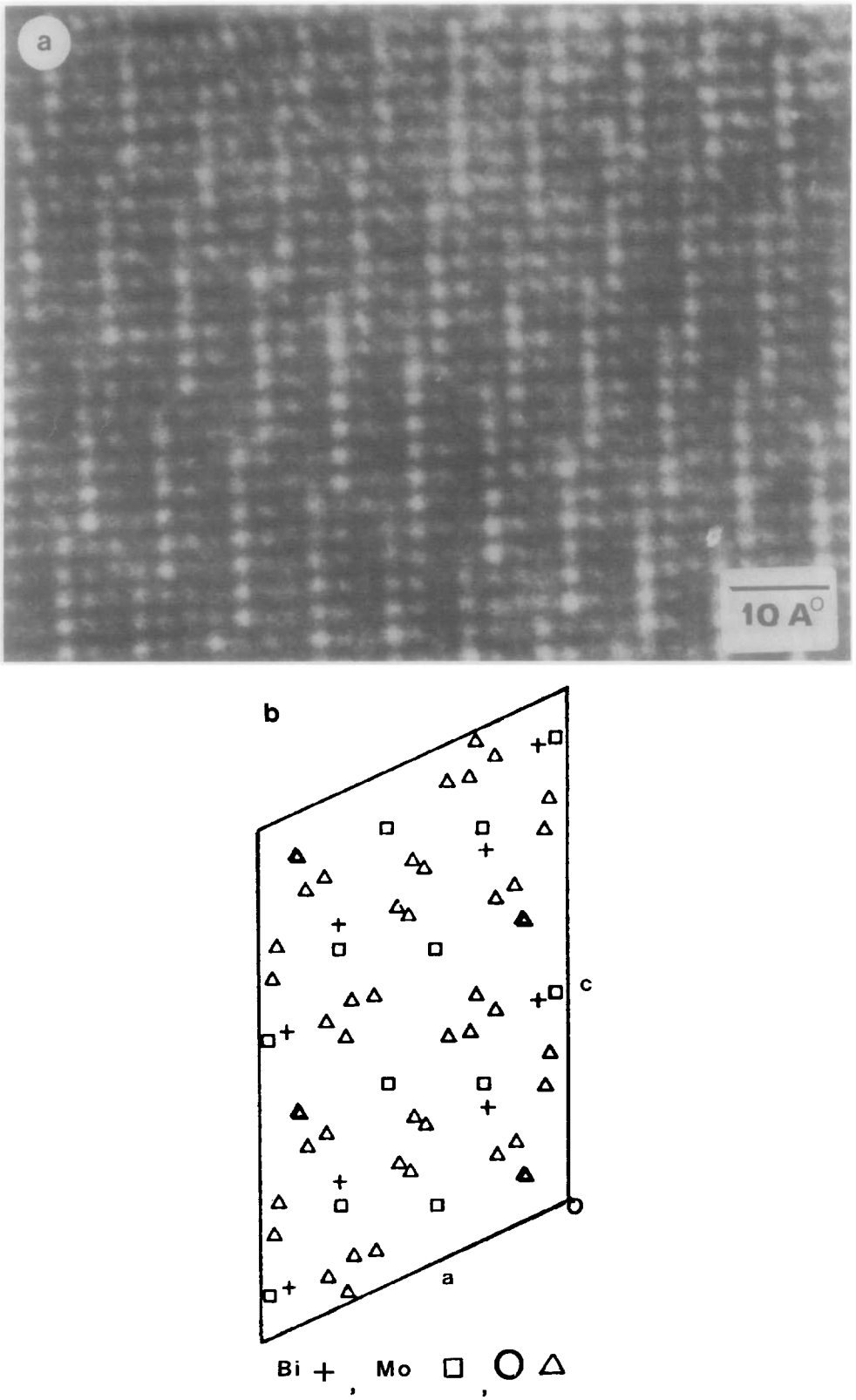

FIG. 4. (a) High resolution image of α-$Bi_2Mo_3O_{12}$ in (010) projection. (b) Atomic projection within the unit cell in (010).

α and Bi_2O_3, etc., as described earlier. Sample B showed mainly tetragonal and γ phases with small amounts of β. HREM examination revealed complex twin lamellae/domains in the tetragonal phase bounded by twin dislocations (*20a,b*), not observed in the fresh preparations. In sample C, together with these phases, β and α as well as a structure with the dimensions ~5.6 × 22 × 17 Å (probably that of γ''; Ref. (*21*)) were detected. Metallic bismuth confirmed by electron diffraction and microanalysis was found in samples B and C. Sample D revealed more metallic Bi and MoO_2. The observations suggest that the activity stages are probably connected to the variations in stoichiometry. Reoxidation of sample C carried out by passing pure oxygen gas showed the presence of α and γ phases as well as Bi_2O_3 and MoO_3, suggesting that some of the changes were reversible. The sample reduced for longer periods (several hours in C_3H_6) also showed transformation of some γ crystallites to the tetragonal phase as shown in Fig. 6.

In Situ Electron Microscopy

Dynamic observations were conducted on single-phase crystallites (several micrometers in size) from the powdered preparations of α and γ, the results of which are summarized below:

α-$Bi_2Mo_3O_{12}$. The (010) samples were reduced in C_3H_6 from room temperature (R.T.) to ~550°C. At an operating temperature of ~440°C, an ordered superlattice was frequently observed in the diffraction pattern giving superlattice spacings of ~8.4 × 10.8 Å. Figures 7a–d illustrate the sequence of reduction in C_3H_6 with (a) the sample at R.T., (b) its diffraction pattern, (c) the sample at 440°C showing crystallites, and (d) the corresponding diffraction pattern with a superlattice of ~8.4 × 10.8 Å. The crystallites were initially nucleated in a few minutes at the surface of the sample confirmed by stereomicroscopy and extended to the subsurface layers/bulk by further reduction. This intermediate phase was somewhat unstable outside the reducing conditions, in air, but it was possible to stabilize it for short periods by an annealing procedure inside the electron microscope so that microanalysis could be carried out. Microanalysis of the crystallites after prolonged reduction indicated a Bi : Mo ratio of ~1 : 1 as shown in the WDS in Fig. 8a. The results of quantitative analysis of the atomic concentrations for the spectrum (a) are shown in (b). Over 20 iterations were carried out in the quantitative microanalysis. The oxygen content was analyzed by difference and the unit was deduced to be close to $Bi_2Mo_2O_9$. Some MoO_3 crystallites were also observed by electron diffraction. Metallic bismuth was detected in the reduced samples by electron diffraction (rings in Fig. 7d, indicated by arrows) and complemented by microanalysis. At ~500°C, more Bi as well as MoO_2 was observed. The observations were confirmed by parallel studies.

γ-Bi_2MoO_6. The (001) samples were reduced as above. Changes at the surface were observed from ~250°C, and near the operating temperature of ~400°C, the samples exhibited a superstructure similar to that observed in α with the spacings of ~8.4 × 10.8 Å. The sequence of reaction is shown in Fig. 9 with (a) the sample at R.T., (b) the corresponding diffraction pattern, (c) the sample at ~400°C with "crystallites" nucleated after ~2 min in the sample,

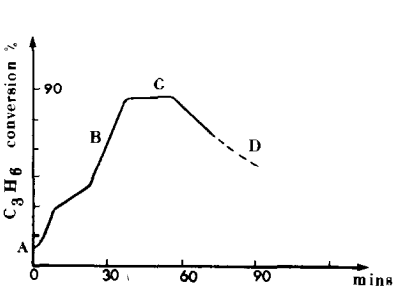

FIG. 5. Isotherm of C_3H_6 conversion on γ-Bi_2MoO_6 system. C_3H_6 is pulsed at intervals of 5–6 min.

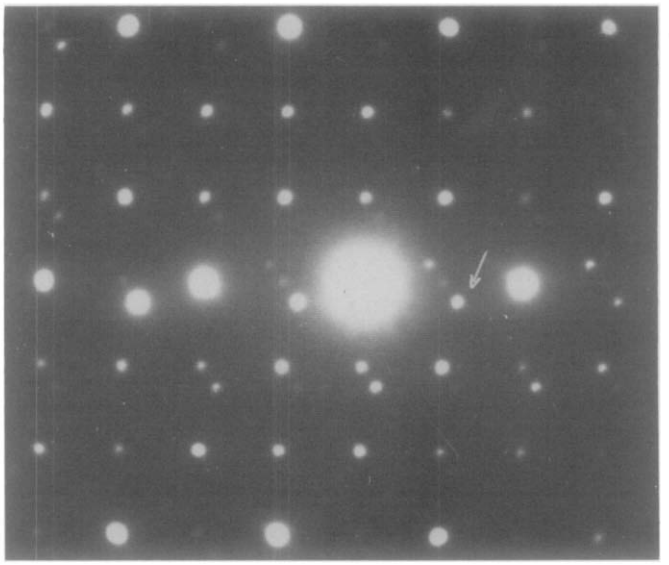

FIG. 6. Transformation of (Bi_2MoO_6) to the tetragonal phase in samples reduced for several hours.

and (d) the corresponding diffraction pattern showing the superlattice. The defect crystallites exhibit black–white contrast indicating that they are confined to the surface layers initially which was subsequently confirmed by stereomicroscopy. Their growth with time was somewhat slow. The sample was tilted to the other crystallographic zones to obtain additional information about the superlattice. AEM indicated the presence of a Bi : Mo ratio of ~1 : 1 in the reacted crystallites. Metallic bismuth crystallites (~0.5 to 1 μm in size) were observed at ~500°C (confirmed by electron diffraction and microanalysis) together with some MoO_2.

In the dynamic experiment using C_3H_6–O_2 mixtures (with a 1 : 1 ratio) both α and γ exhibited the same superstructure at ~400–440°C as in reduction which was reoxidized. The process of reduction to Bi metal, however, was somewhat slowed by the presence of gaseous oxygen.

Experiments conducted on the samples using C_3H_6–O_2 mixtures in the GC–MS for several days showed the presence of degradation products like Bi, MoO_2, etc., but coking was substantially reduced.

Discussion

Observations in the electron microscope of the samples treated in the microreactor have shown that the coprecipitated preparations are multiphase systems with each of the phases detected undergoing microstructural changes during the reactions. From the GC–MS experiments it was possible to produce acrolein (C_3H_4O) and CO_2, etc., with C_3H_6 on the catalyst without gaseous oxygen, suggesting abstraction of lattice oxygen. Under the reducing conditions employed, there is a large driving force for this process and oxygen vacancies are created. The anion vacancies probably exist in low concentrations and are important in understanding oxygen mobility since diffusion is thought to occur via oxygen vacancies. This aspect will be discussed again in the following paragraphs.

The dynamic observations on α and γ

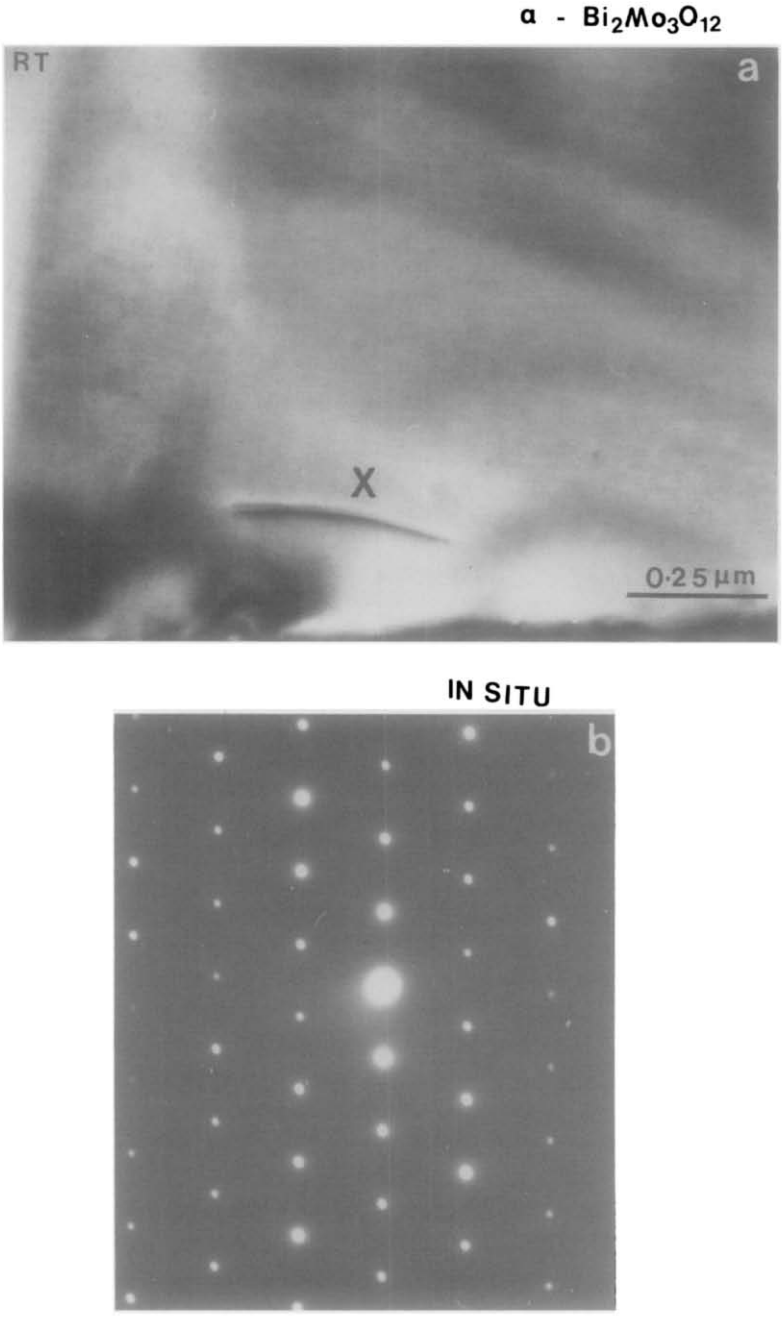

FIG. 7. *In situ* reduction of $Bi_2Mo_3O_{12}$ (area around X): (a) sample at R.T. (b) Diffraction pattern. (c) Sample showing crystallites at 440°C (near the operating temperature). (d) Corresponding diffraction pattern with the superlattice.

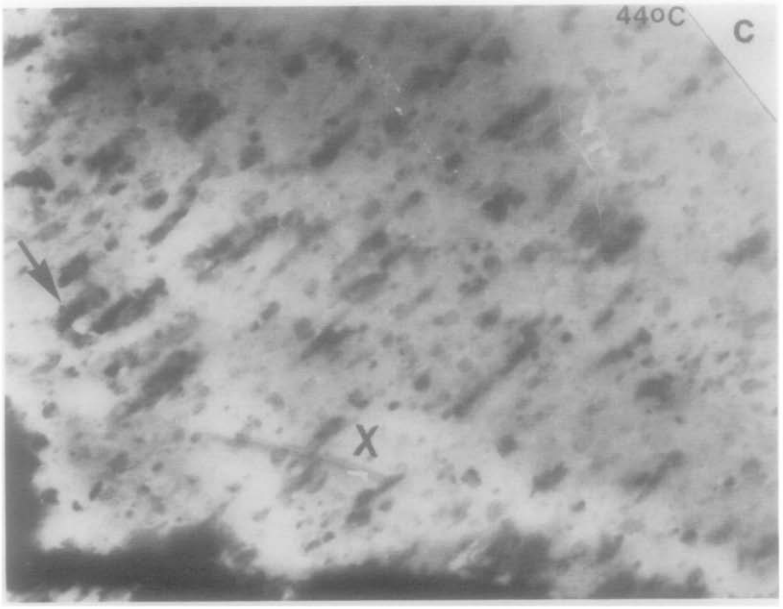

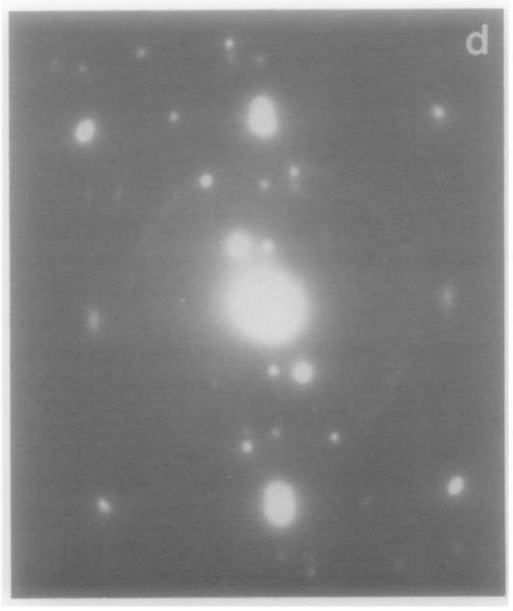

FIG. 7—*Continued.*

have frequently shown the presence of an ordered, intermediate superlattice with dimensions of ~8.4 × 10.8 Å, and the microanalysis has indicated the presence of $Bi_2Mo_2O_9$ in the reacted materials. These observations were confirmed by parallel experiments conducted in the GC–MS system as described earlier. In the light of these

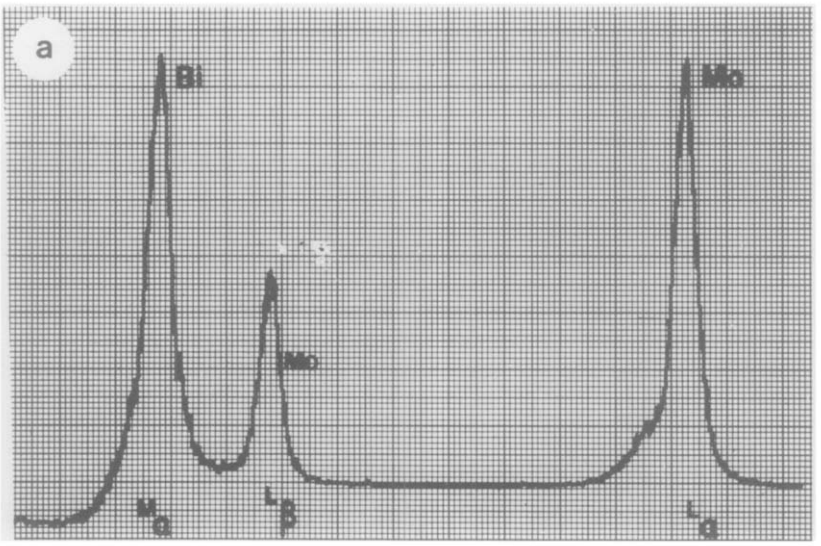

b

ELEMENT	POSITION	PEAK	BACKGR.	K.RATIO
MO	61820.	962.3	15.2	0.2318
BI	58502.	1314.7	101.3	0.4904
TOTAL :				0.7222

ELEMENT	K I.X./I.STD.	K.RATIO	CONCEN.	ATOM. C	
MO :	0.2318	0.2318	0.2460	0.1389	
BI :	0.4904	0.4904	0.5410	0.1402	
O			0.2130	0.7209	BY DIFFERENCE

FIG. 8. Wavelength dispersive spectrometry (WDS) of the crystallites (WDS was also used in conjunction with EDS since in the EDS overlapping of Bi and Mo peaks was observed and for greater precision). (a) Qualitative spectrum. (b) Quantitative analysis of the spectrum shown in (a).

observations it was thought necessary to examine diffraction properties of $Bi_2Mo_2O_9$ (β phase) and pure β samples were prepared by solid state fusion of bismuth oxide (Bi_2O_3) and molybdenum trioxides.

Diffraction patterns as well as lattice images were recorded in, e.g., (100), (101), and (001) projections. The diffraction pattern and lattice image of (101) β are shown in Figs. 10a and b, respectively, and are consistent with the dimensions of the superlattice observed in the *in situ* experiments at operating temperatures, thus suggesting that the superstructure observed is closely related to (101) $Bi_2Mo_2O_9$.

In the fusion preparation of β a small amount of α was also detected by electron microscopy. The coprecipitated preparation showed β as well as large amounts of γ and tetragonal phases.

The structure of β-$Bi_2Mo_2O_9$ has not been solved completely due to its complex na-

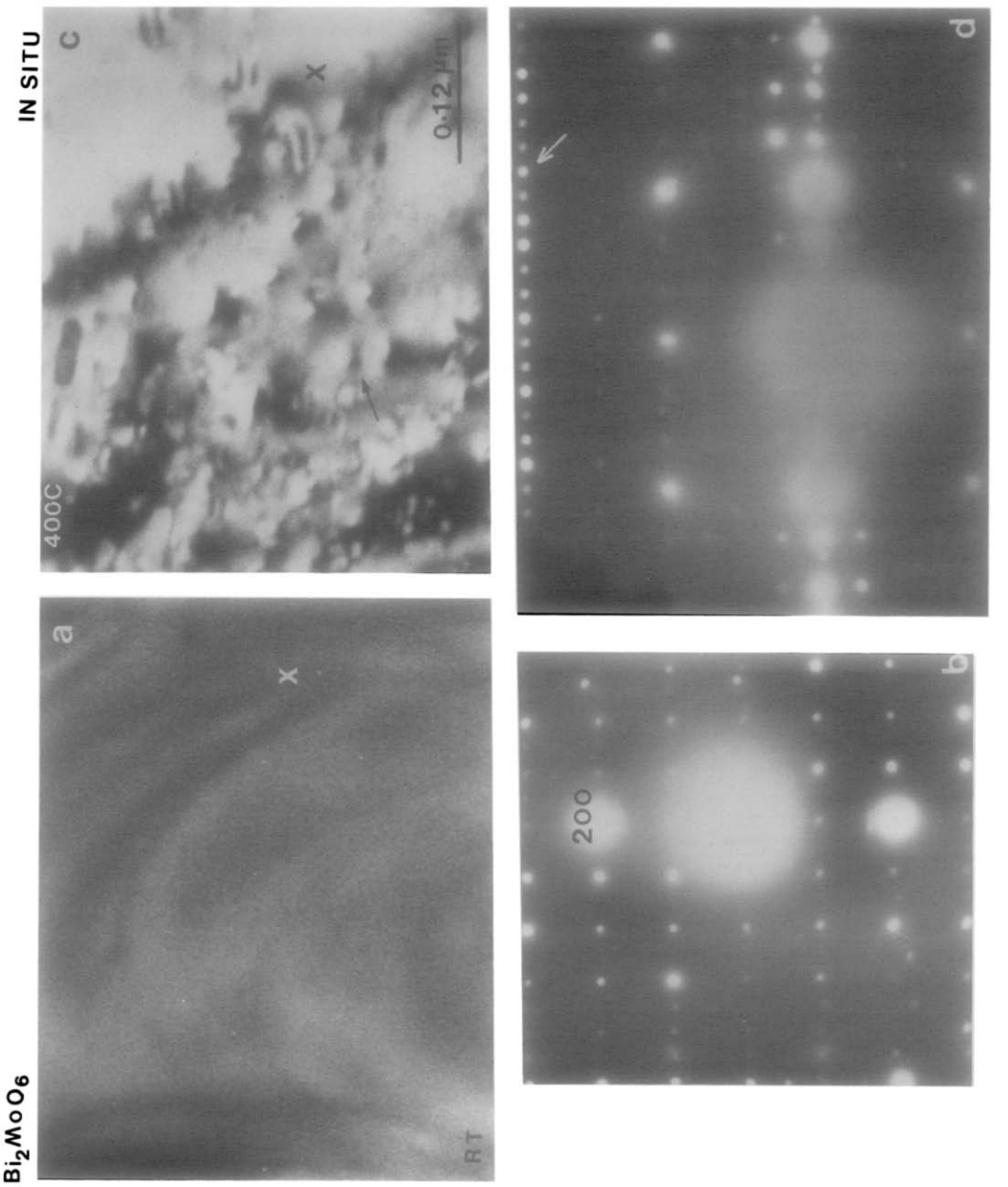

FIG. 9. *In situ* reduction sequence in C_3H_6 of γ-Bi_2MoO_6. (a) Sample at R.T. (b) diffraction pattern. (c) Sample at ~400°C with crystallites (nuclei). (d) Diffraction pattern showing superlattice (Bi_2MoO_6) reflections can also be seen, indicated by arrows).

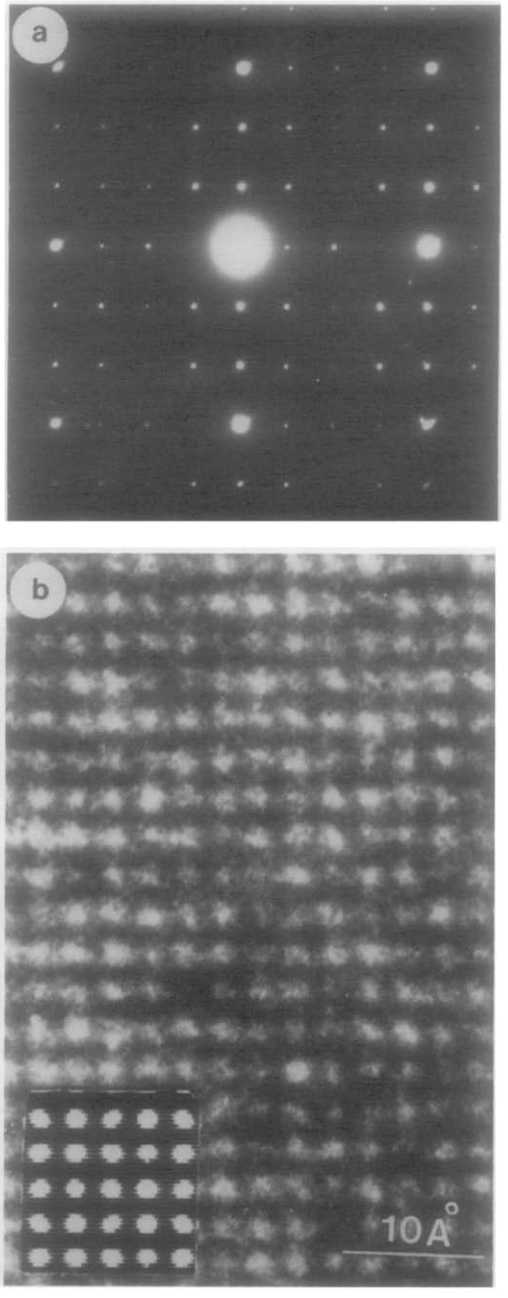

FIG. 10. Images of $Bi_2Mo_2O_9$ at high resolution. (a) (101) diffraction pattern. (b) (101) image of $Bi_2Mo_2O_9$ with the simulated image inset.

ture but an outline model based on the powder diffraction is given by Van den Elzen and Rieck (*22*).[1] The unit cell is large with $a = 11.946$ Å, $b = 10.759$ Å, $c = 11.876$ Å, $\beta = 90.15°$ with space group of the type $P2_1/n = P2_1/C$ and eight formula units. Bi^{3+} is coordinated to eight oxygens and Mo^{6+} is tetrahedrally coordinated. The structure thus contains elements derived from α and γ structures. The tetrahedra are distorted and the cations, together with four Bi vacancies, are distributed within the unit cell. The outline model of the structure due to Van den Elzen and Rieck (*22*) is shown in Fig. 11a.

Differences of opinions exist, however, about the nature of the MoO_4 units, e.g., Van den Elzen and Rieck (*22*) consider all MoO_4 units as equivalent, whereas Matsuura *et al.* (*17*) consider two somewhat different types of MoO_4, one set similar to that in α and the other as in γ. The electron diffraction patterns and the lattice images simulated using the structure data in Ref. (*22*) were found to be in reasonable agreement with the experimental observations. Figure 11b shows the calculated electron diffraction pattern in (101) projection. The (020) type reflections are weak and the rows indicated by the arrows contain weak reflections. The simulated lattice image is inset in Fig. 10b.

The dynamic experiments have shown that both α and γ phases exhibit a similar superstructure in reaction with propylene. The existence of a common phase when in α or γ thus seems likely. The structure of this phase is perhaps similar to γ but with Bi vacancies thus resembling the β structure.

The structure of α is written, for example, as $\alpha = (Bi_{2/3}\phi_{1/3}Mo)O_4$, where ϕ are bismuth vacancies. The α to β type trans-

[1] A more refined structure of $Bi_2Mo_2O_9$ based on single-crystal X-ray diffraction is to be published by Sleight *et al.* (Dr. A. Sleight, Du Pont, private communication, 1982).

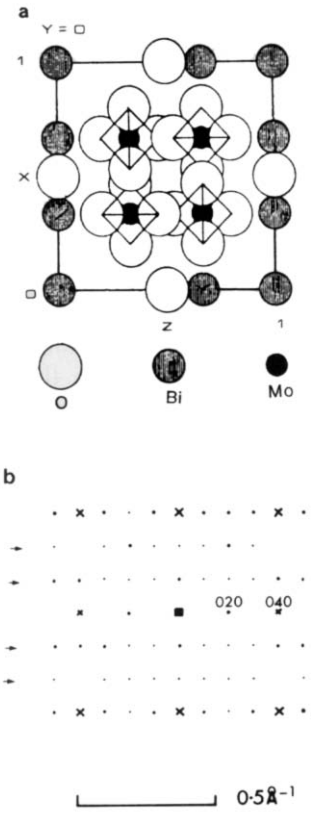

FIG. 11. (a) Structure of $Bi_2Mo_2O_9$. (b) Theoretical electron diffraction pattern.

formation may then occur due to decomposition.

Similarly, the transformation from γ to β-type layers as observed in the experiments may occur either due to decomposition of the compound or, in the presence of excess MoO_3, by suitable rearrangement of cations locally. The presence of metallic bismuth and MoO_2 degradation products was indeed observed in the reactions.

Mechanism

Based on the extensive work in the literature on rate-determining reactions using isotopically labeled propene it is now generally accepted that the first and rate-determining step in olefin oxidation over bismuth molybdate catalysts is the formation of an allylic intermediate following the first hydrogen (α-hydrogen) abstraction. This may be illustrated simply as $CH_2{=}CH{-}CH_3 \xrightarrow{-H} CH_2{\cdots}CH{\cdots}CH_2$.

From GC–MS experiments, as described earlier, lattice oxygen is removed for the olefin oxidation creating anion vacancies. From tracer studies using labeled γ-bismuth molybdates, it is suggested (*23*) that lattice oxygen for the reactions comes from $(Bi_2O_2)^{2+}$ layers whether or not gaseous oxygen is present, and during oxidation the oxide ions consumed are replenished by the diffusion of O^{2-} formed from gaseous oxygen dissociatively chemisorbed, through (MoO_2) layers. It is also now generally believed that the olefin and oxidation adsorption sites are different on the molybdates, i.e., the catalyst reduction and reoxidation occur at different sites. Differences exist, however, as to the nature of the sites, e.g., Sleight (*19*) suggests that olefin chemisorption and α-H abstraction occur via Mo units, whereas olefin chemisorption and α-H abstraction involve Bi cations and Mo polyhedra participate in the insertion of oxygen according to Haber and Zilkowski (*24*). Burington *et al.* (*25*) suggest that α-H abstraction occurs at Bi sites (*A* sites) and Mo participate in olefin chemisorption and oxygen insertion.

The occurrence of the $Bi_2Mo_2O_9$ superstructure at operating temperatures in the reactions studied and the enhanced catalytic activity in its presence constitute important observations. Based on the above discussion (e.g., Refs. (*24, 25*)), it appears that β has a favorable balance of chemisorption sites (Mo) and hydrogen abstraction sites (Bi). From X-ray photoelectron spectroscopy (XPS) of the surfaces of γ, with α mixtures, Matsuura *et al.* (*17*) suggested the Bi : Mo ratio to be near to 1 : 1 (as in the case of β) and attributed the enhanced catalytic activity of the nonstoi-

chiometric bismuth molybdates enriched with Mo to the presence of the compound β. The dynamic experiments presented here conducted on individual phases support the existence of β at operating temperatures and suggest that γ and α can be active under these conditions. The role of bismuth vacancies in the reactions, however, is not clear at the present time. Bi_2O_3 and MoO_3 taken individually, have few chemisorption sites and hydrogen abstraction sites, respectively, and could perhaps explain their inferior activity. Nevertheless, the small amounts of Bi_2O_3, MoO_3, and the tetragonal-2BiMo phase present in the catalyst system undergo microstructural changes during the reactions following the loss of oxygen as observed by electron microscopy and the GC–MS experiments. For example, the conversion of propylene on Bi_2O_3 at temperatures between 400 and 500°C is shown to yield C_6 olefinic products, e.g., hexadiene, and also acrolein, some dehydromerization products, and CO_2 before reducing to bismuth metal (*27, 28*). Furthermore, microstructural changes (e.g., domains and crystallographic shear planes) were also observed in the MoO_3 crystallites before reduction to MoO_2. The analyses of the various defect structures between room temperature and 600°C (including the operating temperatures of ~300–400°C) in the dynamic studies conducted on MoO_3 have been described by Gai (*6*).

Conclusions

In situ electron microscopy studies in combination with high resolution microscopy and microanalytical techniques have provided valuable insight into the microstructure of bismuth molybdates. The results from reactions with propylene suggest formation of an ordered intermediate phase at operating temperatures and that the catalyst selectivity is associated with a particular phase. Additional information about point defects or clusters if any, prior to ordering, may be obtained by energy filtering or diffuse imaging methods or by using higher resolution.

In these commercially important bismuth molybdate catalyst phases studied evidence for extended defects such as crystallographic shear planes was not obtained at catalyst operating temperatures as was also found in the case of industrial tellurium molybdate oxidation catalysts (*12*).

The observations are relevant to one of the crucial points in heterogeneous catalysis, i.e., the role of extended defects such as shear planes in fast diffusion of oxygen, and suggest that shear planes are less relevant or not necessary in some industrial catalytic reactions. It may, therefore, be advantageous to examine the electronic structure of the catalysts more closely, in conjunction with the microstructural studies in such selective oxidation reactions. Attempts are being made to apply imaging and microanalytical techniques normally used for semiconductor materials, such as the cathodoluminescence methods, to the catalysts to examine energy states associated with, e.g., promoters and point defect concentrations (*29, 30*).

Acknowledgments

Grateful thanks are due to Professor Sir Peter Hirsch F.R.S for the provision of Laboratory facilities; SERC (U.K.) for financial support; Dr. E. D. Boyes, Dr. C. J. Salter, and Mr. R. C. Doole for assistance with the Oxford STEM, the Cameca microprobe, and the HVEM; Dr. A. Sleight (Du Pont), Dr. R. K. Grasselli (Sohio), and members of the ICI (heavy chemicals) for interesting discussions; Professor G. D. Rieck of the Eindhoven Institute of Technology, the Netherlands, and Pergamon Press, Oxford, for permission to use Fig. 11a; The Division of Mineralogy, The Smithsonian Institution Washington, D.C., for kindly donating koechlinite samples.

References

1. C. R. ADAMS AND T. J. JENNINGS, *J. Catal.* **2,** 63 (1963).
2. D. J. HUCKNALL, "Selective Oxidation of Hydrocarbons," Academic Press, New York (1974).
3. PH. A. BATIST, J. BOUWENS, AND G. C. SCHUIT, *J. Catal.* **25,** 1 (1972).
4. T. CHEN AND G. C. SMITH, *J. Solid State Chem.* **13,** 288 (1975).
5. P. SWANN AND N. TIGHE, *Jernkont. Ann.* **155,** 479 (1971).
6. P. L. GAI, *Philos. Mag.* **43**(4), 841 (1981).
7. W. THOENI, P. L. GAI, AND P. B. HIRSCH, *J. Less-Common Met.* **54,** 263 (1977).
8. PH. A. BATIST, H. J. PRETTE, AND G. C. SCHUIT, *J. Catal.* **15,** 281 (1969).
9. E. D. BOYES, E. WATANABE, A. J. SKARNULIS, J. L. HUTCHISON, P. L. GAI, M. L. JENKINS, AND M. NARUSE, Institute of Physics (London), Conf. Series 52, Chap. 10, p. 445 (1980).
10. A. J. SKARNULIS, *J. Appl. Crystallogr.* **12,** 636 (1979).
11. E. D. BOYES AND P. L. GAI, "Analytical Electron Microscopy" (R. Geiss, Ed.), San Francisco Press, San Francisco, 71 (1981).
12. P. L. GAI, E. D. BOYES, AND J. C. J. BART, *Philos. Mag. A* **45**(3), 531 (1982).
13. J. ZEMANN, *Heidelb. Beitr. Mineral. Petrogr.* **5,** 139 (1956).
14. A. F. VAN DEN ELZEN AND G. D. RIECK, *Acta Crystallogr. Sect. B* **29,** 2433 (1973).
15. G. BLASSE, *J. Inorg. Nucl. Chem.* **28,** 1124 (1966).
16. V. L. GUNNAR SILLEN AND K. LUNDBORG, *Z. Anorg. Chem.* **252,** 2 (1943).
17. I. MATSUURA, R. SCHUIT, AND K. HARAKAWA, *J. Catal.* **63,** 150 (1980).
18. A. F. VAN DEN ELZEN AND G. D. RIECK, *Acta Crystallogr. Sect. B* **29,** 2436 (1973).
19. A. SLEIGHT, *in* "Advanced Materials in Catalysis" (J. J. Burton and R. L. Garten, Eds.), p. 181, Academic Press, New York (1977).
20. (a) P. L. GAI, *in* "Proceedings, IV International Conference on Mo Chemistry, Colorado School of Mines" (Barry and Mitchell, Eds.), Climax (1982). (b) P. L. GAI, *in* "Proceedings, 40th Electron Microscopy Society of America (EMSA), Washington, D.C. (G. W. Bailey, Ed.), p. 640, Claitors Pub., Baton Rouge (1982).
21. L. YA. ERMAN, E. L. GALPERIN, AND B. P. SOBOLEV, *Russ. J. Inorg. Chem.* **16**(2), 258 (1971).
22. A. F. VAN DEN ELZEN AND G. D. RIECK, *Mater. Res. Bull* **10,** 1163 (1975).
23. H. MIURA, T. OTSUBO, T. SHIRASAKI, AND Y. MORIKAWA, *J. Catal.* **56,** 84 (1979).
24. J. HABER AND J. ZILKOWSKI, *in* "Proceedings, 7th Symp. on Reactivity of Solids, Bristol," Chapman & Hall, London (1973).
25. J. BURINGTON, C. T. KARTISEK, AND R. K. GRASSELLI, *J. Catal.* **63,** 235 (1980).
26. A. SLEIGHT AND W. J. LINN, *Ann. N.Y. Acad. Sci.* **272,** 22 (1976).
27. F. E. MASSOTH AND D. A. SCARPIELLO, *J. Catal.* **21,** 225 (1971).
28. H. E. SWIFT, J. E. BOZIK, AND J. A. ONDREY, *J. Catal.* **22,** 212 (1972).
29. E. D. BOYES, P. L. GAI, D. B. DARBY, AND C. WARWICK, *in* "Proceedings, 40th EMSA, Washington D.C.," (G. W. Bailey, Ed.), p. 664, Claitors Pub., Baton Rouge (1982).
30. E. D. BOYES, P. L. GAI, AND C. WARWICK, to be published.